# Very high-order asymptotic-preserving schemes for hyperbolic systems of conservation laws with parabolic degeneracy on unstructured meshes

Florian Blachère, Christophe Chalons, Rodolphe Turpault

# Very high-order asymptotic-preserving schemes for hyperbolic systems of conservation laws with parabolic degeneracy on unstructured meshes

Florian Blachère[a,*], Christophe Chalons[b], Rodolphe Turpault[c]

[a] *Université de technologie de Troyes, GAMMA3, 12 rue Marie Curie, 10004 Troyes Cedex, France*
[b] *Laboratoire de Mathématiques de Versailles, UMR 8100, Université de Versailles Saint-Quentin-en-Yvelines, UFR des Sciences, bâtiment Fermat, 45 avenue des Etats-Unis, 78035 Versailles Cedex, France*
[c] *Bordeaux-INP, Institut de Mathématiques de Bordeaux, 351 cours de la Libération Bât A33, 33405 Talence Cedex, France*

**Abstract**

In this paper, we consider the numerical approximation of hyperbolic systems of conservation laws with stiff source terms and parabolic degeneracy in the asymptotic limit. We are more precisely interested in the design of high-order asymptotic-preserving schemes on unstructured meshes. Our approach is based on a very simple modification of the numerical flux associated with the usual HLL scheme and boils down to a sharp control of the underlying numerical diffusion. The strategy allows to capture the correct asymptotic parabolic behavior and to preserve the high-order accuracy also in the asymptotic limit. Numerical experiments are proposed to illustrate these properties.

*Keywords:* asymptotic-preserving schemes, diffusion limit, nonlinear hyperbolic systems, high order finite volumes schemes. AMS : 35L50, 65M08

## 1. Introduction

We are interested in the numerical approximation of the solutions to nonlinear hyperbolic systems of conservation laws with possibly stiff relaxation source terms. Such systems are ubiquitous in many physical applications, like for instance in the modelling of gas dynamics with gravity and friction terms, multiphase flows or radiative transfer. In the case of stiff relaxation

*Corresponding author
*Email addresses:* florian.blachere@utt.fr (Florian Blachère), christophe.chalons@uvsq.fr (Christophe Chalons), rodolphe.turpault@u-bordeaux.fr (Rodolphe Turpault)

source terms and under compatibility conditions with the convective terms, see [1] for more details, such systems may have some typical asymptotic (long-time) behaviors and degenerate into parabolic type equations. The concept of asymptotic-preserving schemes has been introduced in Jin [19], Gosse and Toscani [17] and the aim is to preserve this asymptotic behavior at the numerical level. This means in particular that the consistency and stability of the discretization should be uniform with respect to the stiff parameters, or equivalently they should be preserved also in the asymptotic limit. There is an extensive literature available on this topic and the design of first-order asymptotic-preserving schemes in one space dimension is now well understood, see the recent book [16], the references therein, and without any attempt to be exhaustive and for instance [3], [9]... However, turning now to the multi-dimensional case with high-order accuracy, there is a large gap and only a few numerical techniques have been developed up to our knowledge. As far as the multi-dimensional case is concerned, the 1D algorithms can be easily extended on cartesian grids and admissible meshes, but it is much more difficult on unstructured meshes since most schemes loose consistency in the asymptotic limit in this case. Regarding the high-order extension, the main challenges are to preserve the set of admissible states and the high-order accuracy in the asymptotic limit at the same time. We refer for instance the reader to [5, 2] and the references therein for first-order schemes on unstructured meshes, and to [6, 10] and the references therein for high-order extensions. Note that the literature is now extremely large on the topic and that the proposed numerical strategies may also depend on the type of equations under consideration. Regarding kinetic equations for instance, we can also quote [14, 20, 7, 8]...

It is therefore the purpose of this paper to design a class of high-order and asymptotic-preserving schemes on unstructured meshes for the numerical approximation of nonlinear systems with stiff source terms. The present work extends in some sense the recent contribution [10] devoted to high-order and asymptotic-preserving schemes in one space dimension and for linear systems. The proposed strategy is very simple and consists of a mild modification of the usual HLL scheme originally proposed in [18] and such that the consistency error of the scheme stays uniform with respect to the stiff parameters. As we will see, this approach can be understood as a numerical diffusion reduction technique and is especially well-adapted to the high-order extensions on unstructured meshes.

Throughout this paper, we will consider as a typical example the 2D isentropic Euler model with friction given by

$$\partial_t U + \operatorname{div}(F(U)) = \sigma(U) S(U), \tag{1}$$

where $t$ usually denotes the time variable, $x$ the location in space, and where

we have set

$$U = \begin{pmatrix} \rho \\ \rho u \\ \rho v \end{pmatrix}, \; F(U) = \begin{pmatrix} \rho u & \rho v \\ \rho u^2 + p(\rho) & \rho uv \\ \rho uv & \rho v^2 + p(\rho) \end{pmatrix}, \; S(U) = \begin{pmatrix} 0 \\ -\rho u \\ -\rho v \end{pmatrix}. \quad (2)$$

In the following, we will also use the notation $\mathbf{V} = (u, v)^\top$ for the velocity vector. The friction coefficient $\sigma$ is such that $\sigma(U) = \kappa(\rho) > 0$ and the pressure law is assumed to satisfy $p'(\rho) > 0$, so that the convective system is hyperbolic with eigenvalues given by $\mathbf{V}.\mathbf{n} - c$, $\mathbf{V}.\mathbf{n}$ and $\mathbf{V}.\mathbf{n} + c$, for any vector $\mathbf{n} \in \mathbb{R}^2$ and where the sound speed $c$ is given by $c = \sqrt{p'(\rho)}$. Recall that the characteristic field associated with the two extreme eigenvalues are genuinely nonlinear, while the last one is linearly degenerate. The set of admissible states of this model is

$$\mathcal{A} = \{U = (\rho, \rho\mathbf{V}) \in \mathbb{R}^3, \, \rho > 0\}.$$

It was proved in [4] that when $\kappa t \to +\infty$, this system degenerates into the following diffusion equation

$$\partial_t \rho - \operatorname{div}\left(\frac{p'(\rho)}{\kappa(\rho)} \nabla \rho\right) = 0, \quad (3)$$

with convergence speeds given for $p \geq 2$ by

$$\begin{aligned} \|\partial_x^\beta \rho\|_{L^p} &= \mathcal{O}(1+\sigma t)^{-(1-1/p)-\beta/2} \\ \|\partial_x^\beta \partial_t \rho\|_{L^p} &= \mathcal{O}(1+\sigma t)^{-(1-1/p)-\beta/2-1/2} \\ \|\partial_x^\beta \rho u\|_{L^p} &= \mathcal{O}(1+\sigma t)^{-(1-1/p)-\beta/2-1/2} \\ \|\partial_x^\beta \partial_t \rho u\|_{L^p} &= \mathcal{O}(1+\sigma t)^{-(1-1/p)-\beta/2-1} \end{aligned} \quad (4)$$

The outline of the paper is as follows. In the next Section, we first explain why the classical HLL scheme fails in preserving the asymptitc limit (3) by clearly showing the misleading term, and we propose a simple correction in multiple space dimensions. Section 3 discusses the extension to high-order accuracy and Section 4 illustrates the behaviour of our scheme by considering several numerical experiments.

## 2. First-order numerical scheme

### *2.1. Basic notations*

Let us first introduce some classical notations. We suppose that the computational domain $\Omega \subset \mathbb{R}^2$ is covered by $N$ polygonal cells $K$. We consider $e$, a face of the cell $K$, and we suppose that the following admissibility assumptions are satisfied:

- either there exists a single polygonal cell $L$ such that $e = K \cap L \neq \emptyset$. In this case, $e$ can be either a vertex or a single face of the mesh, and in the case of a single face, we note $e = K \cap L$,
- either $e \subset \partial\Omega$ and in this case we will use the same notation $e = K \cap L$ where $L$ is assumed to be a ghost cell to impose boundary conditions.

We note $|K|$ the area of cell $K$, $\mathcal{E}_K$ the set of interfaces of $K$, $|e|$ the length of the interface of $K$ and $L$ ($e = K \cap L$, $L$ being the neighbour of $K$ by the edge $e$), and $\mathbf{n}_{K,e}$ the unit normal vector to $e = K \cap L$ pointing out of $K$. At last, the perimeter $p_K$ of a cell $K$ is defined by $p_K = \sum_{e=K\cap L \in \mathcal{E}_K} |e|$, and $\delta_K = \frac{|K|}{p_K}$ is the so-called space step of the cell $K$.

### *2.2. The classical HLL scheme*

Before going into the details, we first recall the general framework of first-order explicit finite volume scheme for (1) in several space dimensions. We consider that for all $n$ and $K$, $U_K^n$ represents an approximation of the average value of the exact solution at time $t^n$ and on the volume $K$. Invoking the rotational invariance of the Euler equations, the standard finite volume approach to update the solution from time $t^n$ to time $t^{n+1}$ writes

$$U_K^{n+1} = U_K^n - \frac{\Delta t}{|K|} \sum_{e=\mathcal{E}_K} |e| \mathcal{F}_e \cdot \mathbf{n}_{K,e} + \Delta t \sigma_K S_K. \tag{5}$$

In this scheme, $\sigma_K = \sigma(\mathbf{U}_K^n)$ and $S_K = S(\mathbf{U}_K^n)$ approximate the average of $\sigma$ and $S$ on $K$, and $\mathcal{F}_e$ is a numerical flux which approximates the time integral of the exact flux at the interface $e$. An instance of such a numerical flux is given by classical HLL approximate Riemann solvers [18] such as the Rusanov flux leading to

$$\mathcal{F}_e \cdot \mathbf{n}_{K,e} = \frac{1}{2}\big(F(U_K) + F(U_L)\big) \cdot \mathbf{n}_{K,e} - \frac{b_e}{2}\big(U_L - U_K\big), \tag{6}$$

where $b_e > 0$ denotes an upper bound of the absolute value of all wave speeds at interface $e$. We refer the reader to [18] for more details.

Using now the divergence formula

$$\sum_{e\in\mathcal{E}_K} |e| \mathbf{n}_{K,e} = 0 \iff \sum_{e\in\mathcal{E}_K} |e| \mathcal{F}_K \cdot \mathbf{n}_{K,e} = 0, \tag{7}$$

with $\mathcal{F}_K = \mathcal{F}(U_K, U_K)$ and to be plugged into (5), we get

$$U_K^{n+1} = U_K^n - \frac{\Delta t}{|K|} \sum_{e\in\mathcal{E}_K} |e| (\mathcal{F}_e - \mathcal{F}_K) \cdot \mathbf{n}_{K,e} + \Delta t \sigma_K S_K.$$

Finally, introducing the parameter $w_{K,e} = \frac{|e|}{p_K} > 0$ such that

$$\sum_{e \in \mathcal{E}_K} w_{K,e} = 1,$$

the scheme can be equivalently recast as

$$U_K^{n+1} = \sum_{e \in \mathcal{E}_K} w_{K,e} \left( U_K^n - \frac{\Delta t}{\delta_K} (\mathcal{F}_e - \mathcal{F}_K) \cdot \mathbf{n}_{K,e} + \Delta t \sigma_K S_K \right),$$

which can thus be understood as a convex combination of quasi-1D schemes. As far as the definition of the time step $\Delta t$, we impose the following natural CFL condition,

$$\Delta t \leq \min_{K,e} \frac{\delta_K}{4 b_e + \sigma_K \delta_K}, \tag{8}$$

See for instance [5] in the homogeneous case ($\sigma_K = 0$) and [10] for a rigorous proof of stability in the linear non homogeneous case.

### *2.3. Failure of the classical HLL scheme*

In this section, we aim at proving that the classical HLL scheme fails in preserving the asymptotic behavior of the solutions of (1), which is given by (3) when $\kappa t \to +\infty$. A nice way to do that is to reproduce the limit $\kappa t \to +\infty$ by first considering the diffusion scaling given by $\Delta t \leftarrow \Delta t/\varepsilon$ and $\kappa \leftarrow \kappa/\varepsilon$ in (5) and then letting $\varepsilon$ tend to zero. In this section, we assume for the sake of simplicity that $\kappa$ is constant. After easy manipulations, the scheme (5) first writes:

$$\rho_K^{n+1} = \rho_K^n - \frac{\Delta t}{\varepsilon |K|} \sum_{e \in \mathcal{E}_K} \frac{|e|}{2} \left[ \begin{pmatrix} (\rho u)_K^n + (\rho u)_L^n \\ (\rho v)_K^n + (\rho v)_L^n \end{pmatrix} \cdot \mathbf{n}_{K,e} - b_e \big( \rho_L^n - \rho_K^n \big) \right],$$

$$(\rho u)_K^{n+1} = \left( 1 - \frac{\kappa \Delta t}{\varepsilon^2} \right) (\rho u)_K^n - \frac{\Delta t}{\varepsilon |K|} \sum_{e \in \mathcal{E}_K} \frac{|e|}{2} \left[ \begin{pmatrix} (\rho u^2 + p)_K^n + (\rho u^2 + p)_L^n \\ (\rho u v)_K^n + (\rho u v)_L^n \end{pmatrix} \cdot \mathbf{n}_{K,e} - b_e \big( (\rho u)_L^n - (\rho u)_K^n \big) \right],$$

$$(\rho v)_K^{n+1} = \left( 1 - \frac{\kappa \Delta t}{\varepsilon^2} \right) (\rho v)_K^n - \frac{\Delta t}{\varepsilon |K|} \sum_{e \in \mathcal{E}_K} \frac{|e|}{2} \left[ \begin{pmatrix} (\rho u v)_K^n + (\rho u v)_L^n \\ (\rho v^2 + p)_K^n + (\rho v^2 + p)_L^n \end{pmatrix} \cdot \mathbf{n}_{K,e} - b_e \big( (\rho v)_L^n - (\rho v)_K^n \big) \right].$$

Then, considering the Chapmann-Enskog expansions

$$(\rho \mathbf{V})_K^n = (\rho \mathbf{V})_K^{n,0} + \varepsilon (\rho \mathbf{V})_K^{n,1} + \mathcal{O}(\varepsilon^2),$$

a first identification of the terms in $\varepsilon^{-2}$ yields

$$(\rho u)_K^{n,0} = (\rho v)_K^{n,0} = 0. \tag{9}$$

Using these equalities, an identification of the terms in $\varepsilon^{-1}$ gives

$$(\rho \mathbf{V})_K^{n,1} = -\frac{1}{\kappa}(\nabla_h p)_K, \tag{10}$$

where $(\nabla_h p)_K$ is an approximation of the pressure gradient in cell $K$ and given by

$$(\nabla_h p)_K = \frac{1}{|K|}\sum_{e\in\mathcal{E}_K} |e|\Big(\frac{p_K^n + p_L^n}{2}\Big)\mathbf{n}_{K,e}. \tag{11}$$

Considering now the evolution equation on the density $\rho$, we easily get

$$\rho_K^{n+1} = \rho_K^n - \frac{\Delta t}{|K|}\sum_{e\in\mathcal{E}_K}\frac{|e|}{2}\begin{pmatrix}(\rho u)_K^{n,1} + (\rho u)_L^{n,1}\\ (\rho v)_K^{n,1} + (\rho v)_L^{n,1}\end{pmatrix}\cdot\mathbf{n}_{K,e} + \mathcal{O}(\varepsilon) + \\ + \frac{\Delta t}{|K|}\sum_{e\in\mathcal{E}_K}\frac{|e|}{2}b_e\frac{(\rho_L^n - \rho_K^n)}{\varepsilon}$$

which, using (10) becomes

$$\rho_K^{n+1} = \rho_K^n + \frac{\Delta t}{|K|}\sum_{e\in\mathcal{E}_K}\frac{|e|}{\kappa}\Big[\frac{1}{2}(\nabla_h p)_K + \frac{1}{2}(\nabla_h p)_L\Big]\cdot\mathbf{n}_{K,e} + \mathcal{O}(\varepsilon) + \\ + \frac{\Delta t}{|K|}\sum_{e\in\mathcal{E}_K}\frac{|e|}{2}b_e\frac{(\rho_L^n - \rho_K^n)}{\varepsilon}.$$

It is thus clear that the last term of the right-hand side prevents the limit scheme from being a consistent approximation of the limit equation (3), except of course if the mesh size is small compared to $\varepsilon$ in order to compensate the $1/\varepsilon$ factor. Therefore, the classical HLL scheme (5)-(6) is not asymptotic-preserving. However, it is important to observe that this wrong asymptotic behaviour comes from the diffusion term of the HLL numerical flux. This remark motivates the definition of very simple scheme satisfying the asymptotic preserving and given in the next section.

### *2.4. A very simple asymptotically consistent correction*

The results of the last section allow us to see that the problem comes from the numerical diffusion in the density equation. The convergence of this term towards the diffusion regime is not fast enough to be negligible in comparison with the terms that drive the behavior of the system of equations (1)-(2). In order to fix this problem and to obtain the asymptotic-preserving property, we follow [10] and [9] and propose to replace the classical HLL flux (6) at each interface by

$$\mathcal{F}_e\cdot\mathbf{n}_{K,e} = \frac{1}{2}\big(F(U_K) + F(U_L)\big)\cdot\mathbf{n}_{K,e} - \frac{b_e}{2}\theta_e\big(U_L - U_K\big), \tag{12}$$

where $\theta_e = (\theta_e, 1, 1)^T$, which means that only the first equation on the density $\rho$ is concerned by the modification, and $\theta_e = \mathcal{O}(\varepsilon^{1+\alpha})$ with $\alpha > 0$ in the limit $\varepsilon \to 0$ in order to recover the asymptotic-preserving property by forcing the numerical diffusion to be negligible in the first equation close to the diffusion regime. Indeed, the limit scheme writes in this case (still assuming that $\kappa$ is constant)

$$\rho_K^{n+1} = \rho_K^n + \frac{\Delta t}{|K|} \sum_{e \in \mathcal{E}_K} \frac{|e|}{\kappa} \Big[ \frac{1}{2} (\nabla_h p)_K + \frac{1}{2} (\nabla_h p)_L \Big] \cdot \mathbf{n}_{K,e},$$

which is a consistent approximation of the limit equation (3), without any specific requirement on the mesh. Note that the asymptotic-preserving property is also valid when $\kappa$ is not constant but the pressure gradient in the limit scheme are of course weighted in this case. Therefore, the adjustment proposed here provides a numerical scheme that naturally preserves the asymptotic in the diffusion regime.

At last, notice that at this stage the relation $\theta_e = \mathcal{O}(\varepsilon^{1+\alpha})$ does not provide us with an explicit definition of $\theta_e$, especially because of the use the dimensionless form of the equations and therefore the presence of $\varepsilon$. This motivates to check the asymptotic-preserving property by comparing the continuous convergence speeds given in (4) with their discrete counterparts. With this in mind, we rewrite the proposed scheme in the following form

$$\begin{aligned} \frac{\rho_K^{n+1} - \rho_K^n}{\Delta t} = &- \frac{1}{|K|} \sum_{e \in \mathcal{E}_K} \frac{|e|}{2} \begin{pmatrix} (\rho u)_K^n + (\rho u)_L^n \\ (\rho v)_K^n + (\rho v)_L^n \end{pmatrix} \cdot \mathbf{n}_{K,e} \\ &+ \frac{1}{|K|} \sum_{e \in \mathcal{E}_K} \frac{|e|}{2} b_e \theta_e \big( \rho_L^n - \rho_K^n \big), \end{aligned} \tag{13}$$

$$\begin{aligned} \frac{(\rho u)_K^{n+1} - (\rho u)_K^n}{\Delta t} = &- \kappa \rho u_K^n - \frac{1}{|K|} \sum_{e \in \mathcal{E}_K} \frac{|e|}{2} \begin{pmatrix} (\rho u^2)_K^n + (\rho u^2)_L^n \\ (\rho uv)_K^n + (\rho uv)_L^n \end{pmatrix} \cdot \mathbf{n}_{K,e} \\ &- \frac{1}{2} \Big[ (\nabla_h p)_K + (\nabla_h p)_L \Big]_x + \frac{1}{|K|} \sum_{e \in \mathcal{E}_K} \frac{|e|}{2} b_e \big( (\rho u)_L^n - (\rho u)_K^n \big), \end{aligned} \tag{14}$$

$$\begin{aligned} \frac{(\rho v)_K^{n+1} - (\rho v)_K^n}{\Delta t} = &- \kappa \rho v_K^n - \frac{1}{|K|} \sum_{e \in \mathcal{E}_K} \frac{|e|}{2} \begin{pmatrix} (\rho uv)_K^n + (\rho uv)_L^n \\ (\rho v^2)_K^n + (\rho v^2)_L^n \end{pmatrix} \cdot \mathbf{n}_{K,e} \\ &- \frac{1}{2} \Big[ (\nabla_h p)_K + (\nabla_h p)_L \Big]_y + \frac{1}{|K|} \sum_{e \in \mathcal{E}_K} \frac{|e|}{2} b_e \big( (\rho v)_L^n - (\rho v)_K^n \big), \end{aligned} \tag{15}$$

where we have used the notations

$$(\nabla_h p)_K + (\nabla_h p)_L = \begin{pmatrix} \Big[(\nabla_h p)_K + (\nabla_h p)_L\Big]_x \\ \Big[(\nabla_h p)_K + (\nabla_h p)_L\Big]_y \end{pmatrix}.$$

Using standard Taylor expansions combined with the convergence speeds (4) in the $L^\infty$ norm (see again [4]), we have

$$\begin{aligned}
\frac{(\rho u)_K^{n+1} - (\rho u)_K^n}{\Delta t} &\approx \partial_t(\rho u)(t^n, \mathbf{x}_K) = \mathcal{O}(1+\kappa t)^{-2}, \\
\rho u_K^n &= \mathcal{O}(1+\kappa t)^{-3/2}, \\
\frac{1}{|K|}\sum_{e\in\mathcal{E}_K} \frac{|e|}{2} \begin{pmatrix} (\rho u^2)_K^n + (\rho u^2)_L^n \\ (\rho uv)_K^n + (\rho uv)_L^n \end{pmatrix} \cdot \mathbf{n}_{K,e} &\approx \mathrm{div}(\rho V \otimes V)_x(t^n, x_K) = \mathcal{O}(1+\kappa t)^{-2}, \\
\frac{1}{2}\Big[(\nabla_h p)_K + (\nabla_h p)_L\Big]_x &\approx \partial_x p(t^n, x_K) = \mathcal{O}(1+\kappa t)^{-3/2}, \\
\frac{1}{|K|}\sum_{e\in\mathcal{E}_K} \frac{|e|}{2} b_e\big((\rho u)_L^n - (\rho u)_K^n\big) &\approx \mathrm{div}(\tilde{\nabla}\rho u) = \mathcal{O}(1+\kappa t)^{-2},
\end{aligned}$$

where $\tilde{\nabla}$ is a first-order operator which corresponds to a gradient twisted in the direction $KL$ instead of $\mathbf{n}_{K,e}$ on each interface.
Once these developments are completed, the dominant term can be identified to obtain

$$\rho u = -\frac{1}{\kappa}\partial_x p. \tag{16}$$

The same strategy applies on $\rho v$ to get

$$\rho v = -\frac{1}{\kappa}\partial_y p. \tag{17}$$

Considering now the mass conservation equation (13), we get

$$\begin{aligned}
\frac{\rho_K^{n+1} - \rho_K^n}{\Delta t} &\approx \partial_t \rho(t^n, \mathbf{x}_K) = \mathcal{O}(1+\kappa t)^{-3/2}, \\
\frac{1}{|K|}\sum_{e\in\mathcal{E}_K} \frac{|e|}{2} \begin{pmatrix} (\rho u)_K^n + (\rho u)_L^n \\ (\rho v)_K^n + (\rho v)_L^n \end{pmatrix} \cdot \mathbf{n}_{K,e} &\approx \mathrm{div}(\rho V)(t^n, x_K) = \mathcal{O}(1+\kappa t)^{-3/2}, \\
\frac{1}{|K|}\sum_{e\in\mathcal{E}_K} \frac{|e|}{2} b_e\theta_e\big(\rho_L^n - \rho_K^n\big) &\approx \mathrm{div}(\theta_e\tilde{\nabla}\rho),
\end{aligned}$$

so that a definition of $\theta_e$ such that $\theta_e = \mathcal{O}(1+\kappa t)^{-k}$ for a given $k > 0$ and the leading terms would give

$$\partial_t \rho = -\mathrm{div}(\rho \mathbf{V}),$$

and hence, using (16)-(17) the expected diffusive limit, namely

$$\partial_t \rho = \mathrm{div}\Big(\frac{1}{\kappa}\nabla p\Big).$$

In practice, we will set

$$\theta_e = \frac{1}{1+\kappa t},$$

in order to keep as much numerical diffusion as possible without modifying the convergence speed. Indeed, choosing $k \in (0,1)$ would still give an asymptotic preserving scheme but with a wrong speed of convergence towards the limit.

Note that even if the limit scheme is self-imposed and therefore any target scheme cannot be chosen, it is remarkable that it is directly consistent even on unstructured meshes. We will also see that it is very easy to extend to obtain a uniformly high order scheme.

However, it is worth noting two minor disadvantages in practice. The first one is that the CFL condition (8) is in general more restrictive CFL in general compared to the unmodified scheme. The second one is that due to the definitions of $(\nabla_h p)_K$, the stencil of the limit scheme is wider than usual and can cause checkerboard effects in a regime very close to diffusion. Indeed, it is easily seen in 1D where the diffusion operator is approximated by

$$\frac{\rho_{i+2} - 2\rho_i + \rho_{i-2}}{\Delta x^2}.$$

Hopefully, the checkerboard effect only happens on specific meshes when $\kappa$ is so large that the diffusion limit is reached instantly. Therefore, it is seldom a real issue.

## 3. High-order numerical scheme

This section is devoted to the high-order extension of the numerical scheme. The particular form of correction makes it possible to consider doing so using most conventional techniques. We will focus here on the MOOD method but keeping an arbitrary order. In this context, the high order is achieved through a polynomial reconstruction in each cell. The reconstructed polynomial can then be expressed as follows, considering a generic polynomial degree $d$ on cell $K$

$$\tilde{U}_K(x;d) = U_K + \sum_{|\alpha|=1}^{d} \mathcal{R}_\alpha \Big((x-c)^\alpha - \frac{1}{|K|}\int_K (x-c)^\alpha dx\Big) \tag{18}$$

where $c$ is the centroid of the cell $K$, $\mathcal{R}_\alpha$ are the polynomial coefficients, $\alpha = (\alpha_1, \alpha_2) \in \mathbb{N}^2$ is a multi-index with $|\alpha| = \alpha_1 + \alpha_2$, and $(x-c)^\alpha = (x_1 - c_1)^{\alpha_1} + (x_2 - c_2)^{\alpha_2}$, where $x = (x_1, x_2)$ and $c = (c_1, c_2)$. Notice that

this form of polynomial insures that the following property holds by construction

$$\int_K \tilde{U}_K(x;d)dx = U_K.$$

This property is indeed mandatory to obtain effective orders greater than 3. In order to determine the coefficients $\mathcal{R}_\alpha$, a standard least-square approximation is used on a given compact stencil associated with cell $K$, and the reader is referred for instance to [12] for more details.

Once the reconstructed polynomials are defined on each cell, the following generic high-order (in space) finite volume formula is considered

$$U_K^{n+1} = U_K^n - \frac{\Delta t}{|K|} \sum_{e\in\mathcal{E}_K} |e| \sum_{r=1}^{R} \xi_r \mathcal{F}_{e,r} \cdot \mathbf{n}_{K,e} + \Delta t \sigma_K S_K, \tag{19}$$

with

$$\mathcal{F}_{e,r} \cdot \mathbf{n}_{K,e} = \frac{1}{2}\big(F(U_K^{e,r}) + F(U_L^{e,r})\big) \cdot \mathbf{n}_{K,e} - \frac{b_{e,r}}{2}\theta_{e,r}\big(U_L^{e,r} - U_K^{e,r}\big). \tag{20}$$

In these formulas, $U_K^{e,r}$ and $U_L^{e,r}$ represent the high-order approximations of $U$ obtained by evaluating the in-cell reconstructed polynomials at quadratures points $q_{LR}^{e,r}$ located on the edge $e$. The $\xi_r$ are the $R$ quadrature weights. Obviously, the quadrature formula has to be exact for polynomials up to degree $d$. As far as $\sigma_K$ and $S_K$ are concerned, it is defined by the average of $\sigma$ and $S$ on $K$ using the appropriate quadrature formula. At last, the high-order accuracy in time, is obtained by using a standard Strong Stability Preserving Runge-Kutta method (see [21] for instance).

This results in a high order scheme that can easily be implemented generically by choosing appropriate quadrature rules and suitable reconstruction stencils. It remains to be decided which criteria will be used to correct the numerical results, particularly in the vicinity of discontinuities, in order to obtain a satisfactory numerical approximation. The concept of the MOOD method is to test the prediction of the high order numerical scheme at each time step with respect to these criteria and to *a posteriori* correct the cells that do not validate them by locally recalculating with a lower order scheme (possibly the first order parachute scheme which must therefore verify the criteria). The validation criteria will be recalled for each numerical simulation, but it should be noted that it is always necessary to use at least the PAD (Physical Admissibility Detector) criterion. As its name suggests, it checks whether the prediction belongs to the set of physically admissible states and is therefore essential, otherwise the code may crash.

It now remains to check the asymptotic-preserving character of this high-order extension. In order to do so, one can reproduce exactly the same arguments as in Sections 2.3 and 2.4. More precisely, using the diffusive

scaling and focusing for instance on the first-order accuracy in time (but high-order in space) for the sake of simplicity, (19)-(20) can be recast as

$$\begin{aligned}
\rho_K^{n+1} &= \rho_K^n - \frac{\Delta t}{\varepsilon |K|} \sum_{e\in\mathcal{E}_K} \sum_{r=1}^{R} \frac{|e|}{2} \xi_r \Big[ \begin{pmatrix} (\rho u)_K^{n,e,r} + (\rho u)_L^{n,e,r} \\ (\rho v)_K^{n,e,r} + (\rho v)_L^{n,e,r} \end{pmatrix} \cdot \mathbf{n}_{K,e} - \\
&\quad - b_e \theta_{e,r} \big( \rho_L^{n,e,r} - \rho_K^{n,e,r} \big) \Big], \\
(\rho u)_K^{n+1} &= \Big( 1 - \frac{\kappa \Delta t}{\varepsilon^2} \Big) (\rho u)_K^n - \\
&\quad \frac{\Delta t}{\varepsilon |K|} \sum_{e\in\mathcal{E}_K} \sum_{r=1}^{R} \frac{|e|}{2} \xi_r \Big[ \begin{pmatrix} (\rho u^2 + p)_K^{n,e,r} + (\rho u^2 + p)_L^{n,e,r} \\ (\rho uv)_K^{n,e,r} + (\rho uv)_L^{n,e,r} \end{pmatrix} \cdot \mathbf{n}_{K,e} - \\
&\quad - b_e \theta_{e,r} \big( (\rho u)_L^{n,e,r} - (\rho u)_K^{n,e,r} \big) \Big], \\
(\rho v)_K^{n+1} &= \Big( 1 - \frac{\kappa \Delta t}{\varepsilon^2} \Big) (\rho v)_K^n - \\
&\quad \frac{\Delta t}{\varepsilon |K|} \sum_{e\in\mathcal{E}_K} \sum_{r=1}^{R} \frac{|e|}{2} \xi_r \Big[ \begin{pmatrix} (\rho uv)_K^{n,e,r} + (\rho uv)_L^{n,e,r} \\ (\rho v^2 + p)_K^{n,e,r} + (\rho v^2 + p)_L^{n,e,r} \end{pmatrix} \cdot \mathbf{n}_{K,e} - \\
&\quad - b_e \theta_{e,r} \big( (\rho v)_L^{n,e,r} - (\rho v)_K^{n,e,r} \big) \Big].
\end{aligned}$$

Then, considering again the Chapmann-Enskog expansions

$$(\rho \mathbf{V})_K^n = (\rho \mathbf{V})_K^{n,0} + \varepsilon (\rho \mathbf{V})_K^{n,1} + \mathcal{O}(\varepsilon^2),$$

by an identification of the terms in $\varepsilon^{-2}$ and $\varepsilon^{-1}$ we get $(\rho u)_K^{n,0} = (\rho v)_K^{n,0} = 0$ and $(\rho \mathbf{V})_K^{n,1} = -\frac{1}{\kappa} (\nabla_h p)_K$, where $(\nabla_h p)_K$ still approximates the pressure gradient in cell $K$ but is now given by

$$(\nabla_h p)_K = \frac{1}{|K|} \sum_{e\in\mathcal{E}_K} \sum_{r=1}^{R} |e| \xi_r \Big( \frac{p_K^{n,e,r} + p_L^{n,e,r}}{2} \Big) \mathbf{n}_K, e. \tag{21}$$

Finally, considering the evolution equation on the density $\rho$, the limit scheme is again given by (assuming that $\kappa$ is a constant)

$$\rho_K^{n+1} = \rho_K^n + \frac{\Delta t}{|K|} \sum_{e\in\mathcal{E}_K} \frac{|e|}{\kappa} \Big[ \frac{1}{2} (\nabla_h p)_K + \frac{1}{2} (\nabla_h p)_L \Big] \cdot \mathbf{n}_{K,e},$$

which is a consistent approximation of the limit equation (3), again without any specific requirement on the mesh. Furthermore, this approximation is naturally an high-order one due to the properties of the reconstruction polynomials. Indeed, the MOOD nature of the extension is not required to obtain this property and therefore, as mentioned earlier, other techniques based on polynomial reconstructions (*e.g.* (W)ENO) may be used to extend the scheme to high-order.

A uniformly high order numerical scheme was thus obtained, which preserves both the diffusion asymptotic and the set of admissible states. This scheme is relatively simple to obtain through a correction that does not require any particular implementing effort. The only price to pay is a CFL condition which is slightly more restrictive than the one of the scheme described in [6]. However, this drawback may be overcame by using a slightly coarser mesh due to its uniformly high-order nature (the scheme designed in [6] loses its high-order nature when the friction is large).

## 4. Numerical results

In this section we numerically check the behaviour of our scheme in various situations. Besides, we also compare the new HLL-$\theta$ scheme ((5) with flux (12)) to the classical HLL (scheme (5) with flux (6), i.e. HLL-$\theta$ with $\theta_e = 1$ everywhere) and to the HLL-DLP-AP schemes (from [5, 6]).

For the high-order schemes the proper time integrators are used, more precisely SSPRK$(1,1)$, SSPRK$(2,2)$ and SSPRK$(5,4)$ using the notations of [21] for the $\mathbb{P}0$, $\mathbb{P}1$ and $\mathbb{P}3$ schemes. Where the $\mathbb{P}n$ notation denotes a reconstruction of degree $n$ in (18) using the appropriate quadrature formulas [12].

Let us notice, that to have a proper convergence with the HLL-$\theta$-$\mathbb{P}3$ scheme, we impose $\theta_e = 1$ in the flux of the boundary interfaces.

In the MOOD loop, the PAD (Physical Admissibility Detector) criterion is always enabled to check if the solution lies in the set of admissible state $\mathcal{A}$. To avoid spurious oscillations and to keep smooth extrema the DMP (Discrete Maximum Principle) and u2 criteria may be enabled with the $\mathbb{P}_3$ reconstruction. For more details about criteria, the reader is referred to [13, 11].

### *4.1. Convergence to a manufactured solution*

The aim of the first numerical experiment is to check the convergence with respect to the mesh size. In order to define an exact solution of our system (2), we consider a manufactured solution of the form

$$\begin{aligned} \rho(x,y,t) &= \exp(-(x+y)), \\ (\rho u)(x,y,t) = (\rho v)(x,y,t) &= \frac{\exp(-t)}{k}, \\ p(x,y,t) &= \rho(x,y,t)^{\gamma}, \end{aligned} \tag{22}$$

which corresponds to the following source term

$$\sigma(x,y,t) = \frac{-1}{(\rho u)} \left[ \partial_t(\rho u) + \partial_x p - 2\frac{(\rho u)^2 \partial_x(\rho)}{\rho^2} \right]. \tag{23}$$

With this exact solution, the tests are run with a final time $t_f = 1$. Dirichlet boundary conditions are imposed with the exact solution on each sides of the unit square. The first mesh is composed of triangles created with Gmsh (see [15]), while all the finer meshes used are refinements of the first one.

In Figure 1, the $L^2$-norm of the error on $\rho$ is drawn regarding to the number of cells in the mesh. The left plot corresponds to the choice $k = 20$ in (22) and the right one to $k = 640$. The new HLL-$\theta$ scheme (12) with various polynomial reconstructions ($\mathbb{P}0$, $\mathbb{P}1$, $\mathbb{P}3$) is compared to the classical HLL scheme (6) and the HLL-DLP-AP scheme developed in [5].

In the MOOD loop, only the PAD criterion is used as the solution is very smooth and no spurious oscillations are created with the schemes.

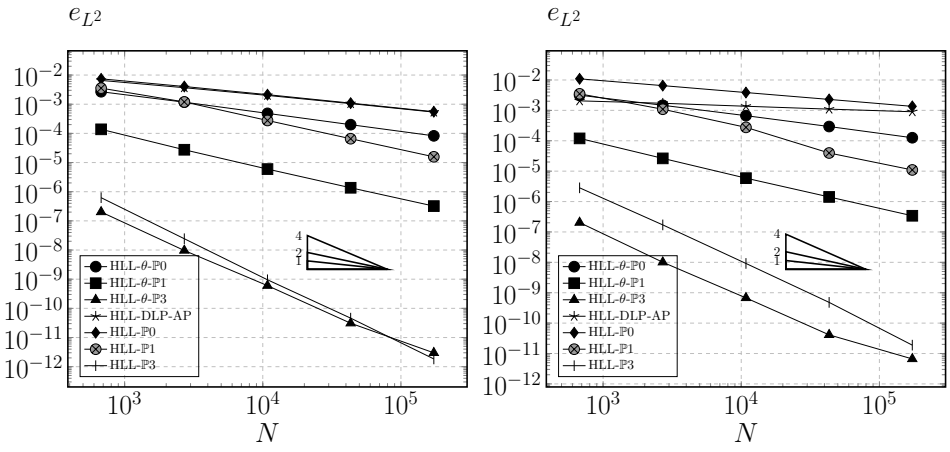


(a) $k = 20$, $\sigma \in [2; 70]$ (b) $k = 640$, $\sigma \in [64; 2600]$

Figure 1: Rate of convergence regarding to the mesh with a manufactured solution (22)

Figure 1 shows a good agreement with the theoretical convergence rates for all the schemes. Besides, the new schemes offer a better convergence rate especially with large source terms.

*4.2. Convergence to the diffusive limit*

The next test case illustrates the behaviour of the numerical schemes with respect to the long time behaviour and the corresponding convergence speeds (4). With this in mind, we plot on Figure 2 the evolution of $\|\rho(t)\|_{L^p}$ and $\|(\rho u)(t)\|_{L^p}$ for $p = 2$ and $p = \infty$ with respect to $1 + \sigma t$.

The initial condition is a Gaussian curve, namely

$$\begin{aligned} \rho_0(x, y) &= \exp\left(-(x - 50)^2 - (y - 50)^2\right) + 1 \\ \mathbf{V}_0(x, y) &= 0. \end{aligned} \tag{24}$$

An unstructured mesh of $[0; 100]^2$ composed of $6.6 \cdot 10^3$ triangles and a space step $\Delta x = \min_K \delta_K = 1.7 \cdot 10^{-1}$ are used. Neumann boundary conditions

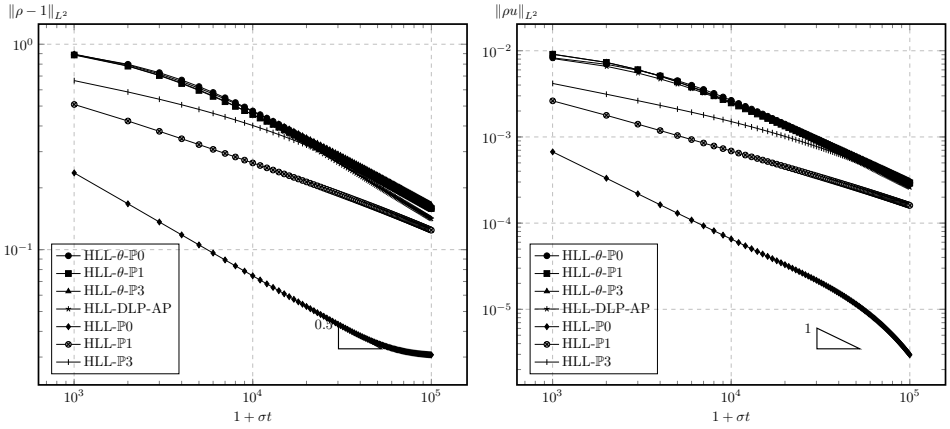


(a) $\|\rho - 1\|_{L^2}$ (b) $\|\rho u\|_{L^2}$

(c) $\|\rho - 1\|_{L^\infty}$ (d) $\|\rho u\|_{L^\infty}$

Figure 2: Decays in time of $\|\rho\|_{L^p}$ and $\|\rho u\|_{L^p}$

are considered. The long time behaviour is observed using a large final time $t_f = 10^3$ and a large (constant) source term $\sigma = 10^2$.

The results are obtained with various schemes (HLL-$\theta$, HLL and HLL-DLP-AP). The high-order schemes only use the PAD criterion in the MOOD loop. We observe that the proposed asymptotic-preserving schemes fully respect the convergence rates whereas the classical HLL scheme gives the correct convergence rate when the high-order reconstructions are used.

### *4.3. Blast with friction*

The last numerical test shows the behaviour of our scheme in a more complex configuration. In the unit square two zones are set: one inside a circle of radius 0.3 centered at $(0.5, 0.4)$ with the following initial condition

$$\rho_0 = 5, \quad \mathbf{V}_0 = 0,$$

and one outside the circle with:

$$\rho_0 = 1, \quad \mathbf{V}_0 = 0.$$

All sides of the square are considered as walls and the source term is controlled by:

$$\sigma(U) = 5\left(\frac{\rho}{5}\right)^3$$

The mesh created with Gmsh is composed of $4 \cdot 10^4$ triangles for a space step of $8 \cdot 10^{-4}$. Finally, the MOOD loop used for the high-order schemes use the PAD, DMP and u2 criteria [13].

The results are presented in Figures 4 and 5 at two final times (0.35 on the left and 0.75 on the right). The HLL-$\theta$-$\mathbb{P}0$ and HLL-DLP-AP-$\mathbb{P}0$ are used in Figure 4 while the Figure 5 shows the results of the HLL-$\theta$-$\mathbb{P}3$ and HLL-DLP-AP-$\mathbb{P}3$. The density values lie in $[0.5; 5.1]$ at time 0.35 and $[1; 3.5]$ at time 0.75.

In order to make the comparison, "reference" solutions obtained on fine meshes of $6 \cdot 10^5$ cells ($\Delta x = 2 \cdot 10^{-4}$) and $2.7 \cdot 10^6$ cells ($\Delta x = 1 \cdot 10^{-4}$) with the HLL-$\theta$-$\mathbb{P}0$ and HLL-$\theta$-$\mathbb{P}3$ schemes, are presented in Figure 3.

For the $\mathbb{P}0$ schemes in Figure 4 the precision is a bit better with the HLL-DLP-AP scheme. Whereas, the HLL-$\theta$-$\mathbb{P}3$ scheme gives a better description of the central structure in Figure 5. This behaviour is expected as HLL-$\theta$ is a true high-order scheme while HLL-DLP-AP only use high-order polynomial reconstruction and get down to a first-order scheme when targeting the limit.

The total run to the final time $t_f = 1$ took $2.2 \cdot 10^4$ iterations and 1h with the HLL-$\theta$-$\mathbb{P}0$ scheme with an average time step of $\Delta t = 4.5 \cdot 10^{-5}$ whereas the HLL-DLP-AP-$\mathbb{P}0$ took $5 \cdot 10^3$ iterations and 2h with $\Delta t = 2 \cdot 10^{-4}$. This difference can be explained as the HLL-DLP-AP scheme use the classical hyperbolic CFL but needs to compute nonlinear coefficients ($\nu$ in [5]) at each time step.

For the $\mathbb{P}3$ schemes the difference between the two computational times is greater (10h and 30h) as there are more coefficients to compute for the HLL-DLP-AP scheme.

In Figure 6, a comparison is made with a reference solution obtained as in [22]. This reference solution is computed with a 1D code using the HLL-$\theta$ scheme from [10] adapted to the isentropic Euler model with friction (2). In order to take account of the cylindrical symmetry of the test case, we added the geometrical source term :

$$S_g(U) = \frac{-1}{r}\begin{pmatrix}\rho \\ \rho u\end{pmatrix}.$$

with $r$ the distance from the center. $10^5$ points are used on the domain $[0; 0.6]$ to model the line $(0.5, 0.4) - (0.5, 1.0)$ from the 2D results. The plots are made at time $t = 0.1$ to preserve the cylindrical symmetry of the test

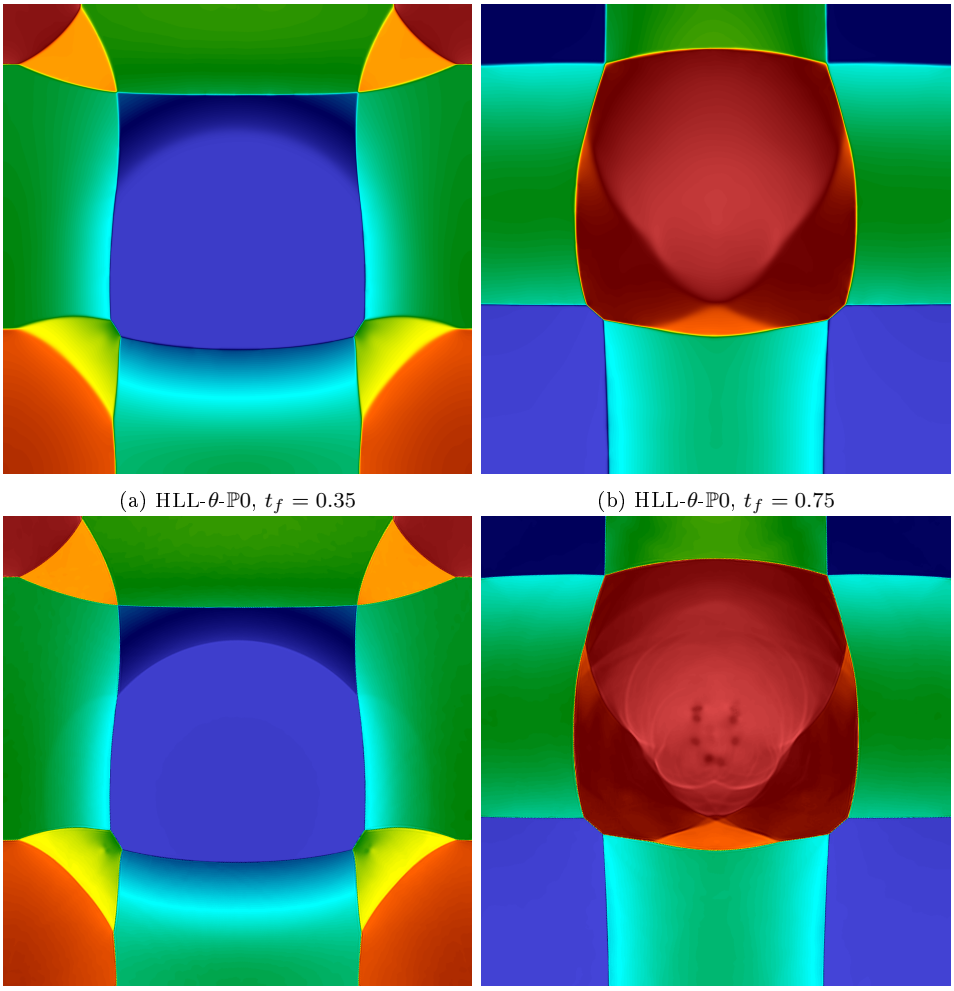

(a) HLL-$\theta$-$\mathbb{P}0$, $t_f = 0.35$ (b) HLL-$\theta$-$\mathbb{P}0$, $t_f = 0.75$

(c) HLL-$\theta$-$\mathbb{P}3$, $t_f = 0.35$ (d) HLL-$\theta$-$\mathbb{P}3$, $t_f = 0.75$

Figure 3: Density results on fine meshes for the blast at various times

case as the waves did not reach the north wall. The time and friction are small so we are mainly checking the improvement of the accuracy of the high-order scheme by comparing the left and right plots. The $\mathbb{P}3$ results present small oscillations as the MOOD criteria (DMP and u2) are not set to be very restrictive. The HLL-$\theta$ and HLL-DLP-AP schemes give nearly the same results as we are close to the hyperbolic regime. However, as written previously, the HLL-$\theta$ is faster because there is no nonlinear coefficients to compute.

## References

[1] C. Berthon, P. G. LeFloch, and R. Turpault. Late-time/stiff-relaxation asymptotic-preserving approximations of hyperbolic equations. *Math.*

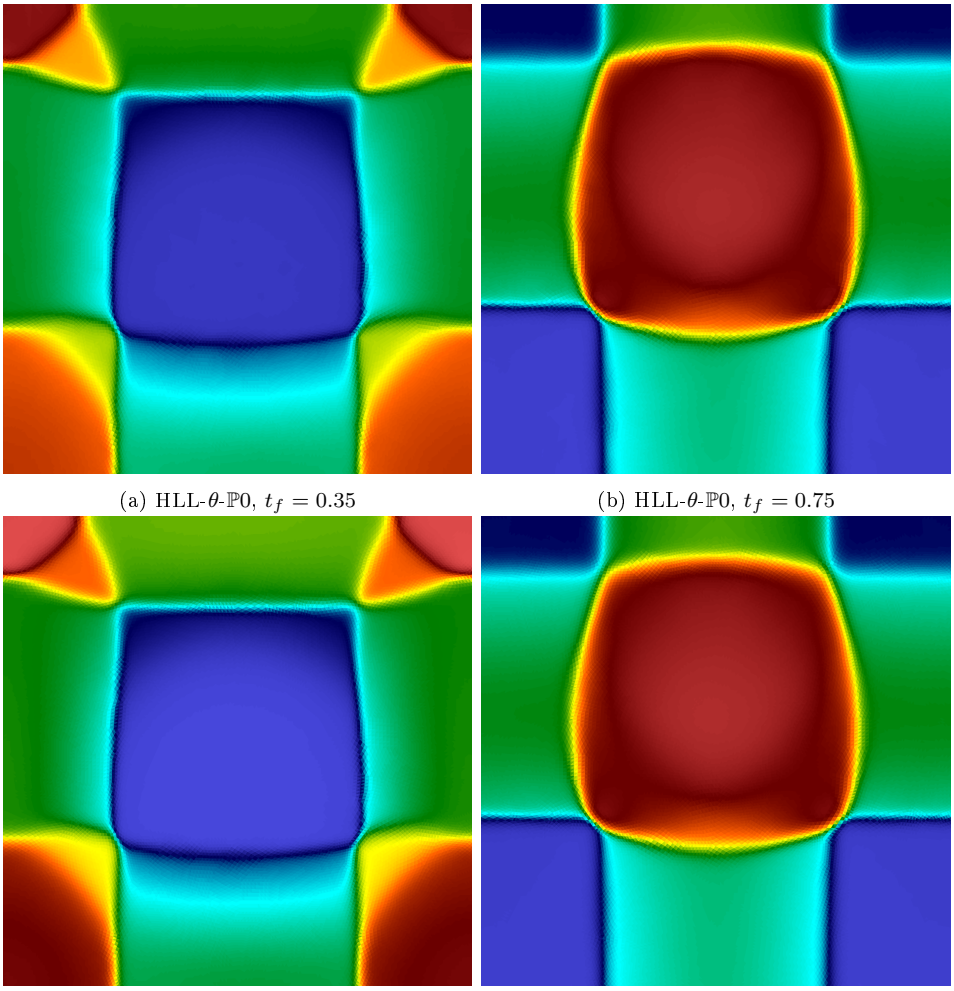

(a) HLL-$\theta$-$\mathbb{P}0$, $t_f = 0.35$ (b) HLL-$\theta$-$\mathbb{P}0$, $t_f = 0.75$

(c) HLL-DLP-AP-$\mathbb{P}0$, $t_f = 0.35$ (d) HLL-DLP-AP-$\mathbb{P}0$, $t_f = 0.75$

Figure 4: Density results for the blast at various times with $\mathbb{P}0$ schemes

*Comp.*, 82(282):831–860, 2013.

[2] C. Berthon, G. Moebs, C. Sarazin-Desbois, and R. Turpault. An asymptotic-preserving scheme for systems of conservation laws with source terms on 2D unstructured meshes. *Commun. Appl. Math. Comput. Sci.*, 11(1):55–77, 2016.

[3] C. Berthon and R. Turpault. Asymptotic preserving HLL schemes. *Numer. Methods Partial Differential Equations*, 27(6):1396–1422, 2011.

[4] S. Bianchini, B. Hanouzet, and R. Natalini. Asymptotic behavior of smooth solutions for partially dissipative hyperbolic systems with a convex entropy. *Comm. Pure Appl. Math.*, 60(11):1559–1622, 2007.

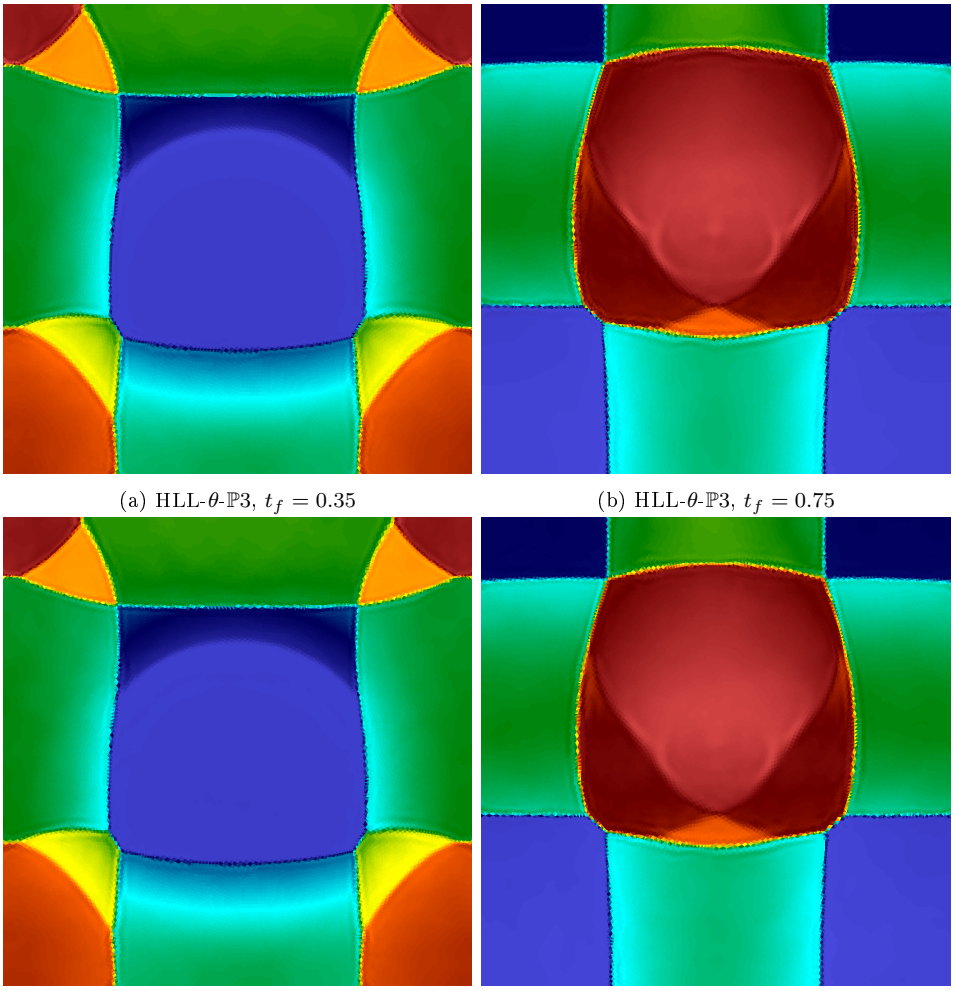

(a) HLL-$\theta$-$\mathbb{P}3$, $t_f = 0.35$ (b) HLL-$\theta$-$\mathbb{P}3$, $t_f = 0.75$

(c) HLL-DLP-AP-$\mathbb{P}3$, $t_f = 0.35$ (d) HLL-DLP-AP-$\mathbb{P}3$, $t_f = 0.75$

Figure 5: Density results for the blast at various times with $\mathbb{P}3$ schemes


[5] F. Blachère and R. Turpault. An admissibility and asymptotic-preserving scheme for systems of conservation laws with source term on 2D unstructured meshes. *J. Comput. Phys.*, 315:98–123, 2016.

[6] F. Blachère and R. Turpault. An admissibility and asymptotic preserving scheme for systems of conservation laws with source term on 2D unstructured meshes with high-order MOOD reconstruction. *Comput. Methods Appl. Mech. Engrg.*, 317:836–867, 2017.

[7] S. Boscarino, P. G. LeFloch, and G. Russo. High-order asymptotic-preserving methods for fully nonlinear relaxation problems. *SIAM J. Sci. Comput.*, 36(2):A377–A395, 2014.

[8] S. Boscarino, L. Pareschi, and G. Russo. Implicit-explicit Runge-Kutta

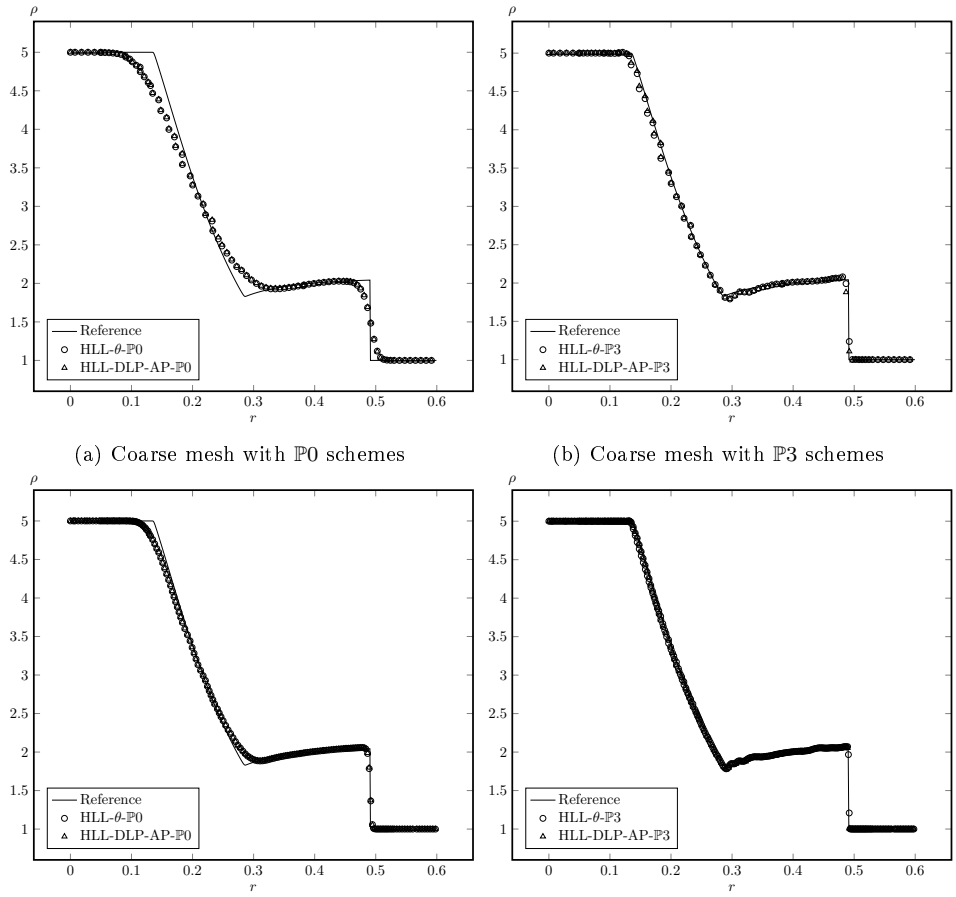


(a) Coarse mesh with ℙ0 schemes

(b) Coarse mesh with ℙ3 schemes

(c) Fine mesh with ℙ0 schemes

(d) Fine mesh with ℙ3 schemes

Figure 6: Density results for the blast at time $t = 0.1$ on the line $(0.5, 0.4) - (0.5, 1.0)$

schemes for hyperbolic systems and kinetic equations in the diffusion limit. *SIAM J. Sci. Comput.*, 35(1):A22–A51, 2013.

[9] C. Chalons, M. Girardin, and S. Kokh. Large time step and asymptotic preserving numerical schemes for the gas dynamics equations with source terms. *SIAM J. Sci. Comput.*, 35(6):A2874–A2902, 2013.

[10] C. Chalons and R. Turpault. High-order asymptotic-preserving schemes for linear systems: Application to the goldstein-taylor equations. *Numer Methods Partial Differential Eq.*, 35:1538–1561, feb 2019.

[11] S. Clain and J. Figueiredo. The MOOD method for the non-conservative shallow-water system. *Comput. & Fluids*, 145:99–128, 2017.

[12] S. Diot. *La méthode MOOD Multi-dimensional Optimal Order Detection: la première approche a posteriori aux méthodes volumes fi-*

*nis d'ordre très élevé*. PhD thesis, Université de Toulouse, Université Toulouse III-Paul Sabatier, August 2012.

[13] S. Diot, S. Clain, and R. Loubère. Improved detection criteria for the multi-dimensional optimal order detection (MOOD) on unstructured meshes with very high-order polynomials. *Comput. & Fluids*, 64:43–63, 2012.

[14] F. Filbet and S. Jin. A class of asymptotic-preserving schemes for kinetic equations and related problems with stiff sources. *J. Comput. Phys.*, 229(20):7625–7648, 2010.

[15] C. Geuzaine and J.-F. Remacle. Gmsh: A 3-D finite element mesh generator with built-in pre- and post-processing facilities. *Internat. J. Numer. Methods Engrg.*, 79(11):1309–1331, 2009.

[16] L. Gosse. *Computing qualitatively correct approximations of balance laws*, volume 2 of *SIMAI Springer Series*. Springer, Milan, 2013. Exponential-fit, well-balanced and asymptotic-preserving.

[17] L. Gosse and G. Toscani. An asymptotic-preserving well-balanced scheme for the hyperbolic heat equations. *C. R. Math. Acad. Sci. Paris*, 334(4):337–342, 2002.

[18] A. Harten, P. D. Lax, and B. van Leer. On upstream differencing and Godunov-type schemes for hyperbolic conservation laws. *SIAM Rev.*, 25(1):35–61, 1983.

[19] S. Jin. Efficient asymptotic-preserving (AP) schemes for some multiscale kinetic equations. *SIAM J. Sci. Comput.*, 21(2):441–454 (electronic), 1999.

[20] P. Lafitte, A. Lejon, and G. Samaey. A High-Order Asymptotic-Preserving Scheme for Kinetic Equations Using Projective Integration. *SIAM J. Numer. Anal.*, 54(1):1–33, 2016.

[21] R. J. Spiteri and S. J. Ruuth. A new class of optimal high-order strong-stability-preserving time discretization methods. *SIAM J. Numer. Anal.*, 40(2):469–491 (electronic), 2002.

[22] E. F. Toro. *Riemann solvers and numerical methods for fluid dynamics*. Springer-Verlag, Berlin, third edition, 2009. A practical introduction.